Biophysical Journal, Volume 99

Supporting Material

Title: Identification of the Third Na^+ Site and the Sequence of Extracellular Binding Events in the Glutamate Transporter

Zhijian Huang and Emad Tajkhorshid

Identification of the Third Na^+ Site and the Sequence of Extracellular Binding Events in the Glutamate Transporter

Zhijian Huang and Emad Tajkhorshid*

Department of Biochemistry,
Beckman Institute, and
Center for Biophysics and Computational Biology,
University of Illinois at Urbana-Champaign,
Urbana, Illinois 61801, U.S.A.

Supporting Material

*Corresponding author: email: emad@life.uiuc.edu; phone: +1-217-244-6914; fax: +1-217-244-6078.

Methods

Membrane modeling of trimeric Glt_{ph}

The simulation system was constructed by embedding a trimeric form of Glt_{ph}, adopted from the crystal structure of the outward-facing Glt_{ph} (PDB code 2NWX (1)) into a lipid bilayer, as described in detail below. Detergent molecules were removed. The coordinates of the missing residues (residues 119 to 127 in one monomer and residues 123 to 127 in the other two monomers) were adopted from the crystal structure of the TBOA-bound state of Glt_{ph} (PDB code 2NWW (1)). The coordinates of the other missing side chains and hydrogen atoms were added by the PSFGEN plugin in VMD (2) employing the CHARMM27 topology files. Water molecules were added to the internal cavities of the protein using DOWSER (3), and the protein was solvated using the SOLVATE program (4). Glt_{ph} trimer was then aligned along the membrane normal using the OPM (Orientations of Proteins in Membranes) database (5), and water molecules in the potential lipid-protein interface were deleted. Solvated Glt_{ph} trimer was then inserted into a patch of POPE (1-palmitoyl-2-oleoyl-*sn*-glycero-3-phosphatidylethanolamine) with the membrane normal along the z-axis. The lipid molecules overlapping with the protein were deleted, resulting in a simulation system with 437 lipids. Additional solvent was added to both sides of the membrane, and the system was neutralized with 100 mM NaCl using the SOLVATE and AUTOIONIZE plugins of VMD (2). The size of the final simulation system is $143\times141\times107$ Å^3 with ∼225,000 atoms.

Simulation protocol

All simulations were performed under periodic boundary conditions with a time step of 1 fs using NAMD 2.6 (6). The TIP3P model for explicit water (7) and the CHARMM27 force field (8) including the CMAP corrections (9) were used. First, lipid tails were melted in a 500-ps NVT (constant volume and temperature) simulation at 303 K during which all other atoms were fixed. The system was then equilibrated in an NPT (constant pressure and temperature) simulation at 1 atm and 303 K for 2 ns during which the heavy atoms of the protein were constrained by harmonic potentials ($k = 2$ kcal/mol/Å^2) to allow the lipid molecules and water to pack around the protein. Next, all the constraints were removed, and the NPT equilibration was continued for additional 2 ns. Finally, the production runs (listed in Table 1) were performed with constant area of the lipid bilayer (the NP_nAT ensemble) with a constant normal pressure (P_n) of 1 atm. Constant temperature was maintained by employing Langevin dynamics with a damping coefficient of 0.5 ps^{-1}. The Langevin piston method (10, 11) was employed to maintain a constant pressure with a piston period of 100 fs. Non-bonded interactions were calculated using a cutoff distance of 12 Å and long-range electrostatic interactions were calculated using the particle mesh Ewald (PME) method (12).

Simulation systems

A summary of the various bound states of Glt_{ph} investigated in this study is given in Table 1. Note that the majority of the simulation systems used to study the binding sequence do not include a Na^+ ion in the Na2 binding site, since our previous study (13) showed that this binding site is the most exposed site and the last one to bind an ion during the extracellular half of the transport cycle. As each monomer functions independently (1, 14, 15), we have taken advantage of the trimeric configuration of the simulation systems, and in some of them modeled individual monomers in different bound states. We emphasize here that all simulations have been performed using trimeric Glt_{ph}. For clarity we refer to the protein-only system, i.e., Glt_{ph} without the substrate and the Na^+ ions, as the *apo* state. Various bound states (*apo*, Na1-bound, substrate-bound and substrate/Na1-bound) were constructed to study equilibrium dynamics of Glt_{ph} and to investigate the solvent accessibility of key residues, in particular that of Asp312 and Asp405, in the presence and absence of the substrate and the Na^+ ions in the Na1 and Na2 sites (Systems S1-S4 in Table 1). Some of the analyses are based on the notion that a Na^+ binding site has to be accessible by water from outside before it can be reached by a Na^+ ion. Each state has been simulated at least three times, e.g., Systems S1-a, S1-b, and S1-c for the *apo* state. Note that the initial protein structure in all the simulations was the occluded state, i.e., the reported crystal structure of the outward-facing state of Glt_{ph} (1), unless specified otherwise.

In order to further probe the putative Na3 site, additional simulations were performed. We removed the Na^+ ion at the Na1 site from the equilibrated structure of the Na1-bound state (at $t = 50\,ns$), and substituted a Na^+ ion for a water molecule randomly selected from the vicinity (3.5 Å) of Asp312, which has been suggested to be involved in Na^+ binding in GlTs (16). In total, five water molecules can be found within this radius, and, thus, five independent simulation systems (Na3-a to Na3-e in Table 1) were constructed. The inserted Na^+ ion was initially constrained harmonically ($k = 2\,kcal/mol/Å^2$) for 0.5 ns, and then released during the following 20 ns of free simulation. In order to improve the statistics, this procedure was repeated, but this time using the equilibrated structure of the Na1-bound state at $t = 40\,ns$ as the starting point, thus, resulting in five additional independent simulations (Na3-f to Na3-j in Table 1). In order to inspect the stability of the putative Na3 site upon simultaneous binding of ions to both the Na1 and Na3 sites, two additional simulations were performed in which a Na^+ ion was added to the Na1 binding site in one of the Na3-bound states obtained from the Na3 simulations (Na3-a – Na3-j) described above. In one of these simulations, the stability of the putative Na3 site was examined, whereas in the second simulation the stability of the intermediate site identified in some of the Na3 simulations (see Results for details) was investigated. Each system was simulated for 20 ns. Furthermore, in order to examine the effect of the D405N mutation on the structure of the Na^+ binding sites and the coordination of the ions, a 30-ns simulation of this mutant in the Na1-bound state was performed. Finally, in order to examine whether a "fully bound" structure, i.e., the one with the substrate and the three Na^+ ions, is stable, starting from the crystal structure of Glt_{ph} (1), that is, the substrate/Na1/Na2-bound state, we added a Na^+

ion to the putative Na3 site identified in our earlier simulations, and simulated the system for 20 ns (Table 1).

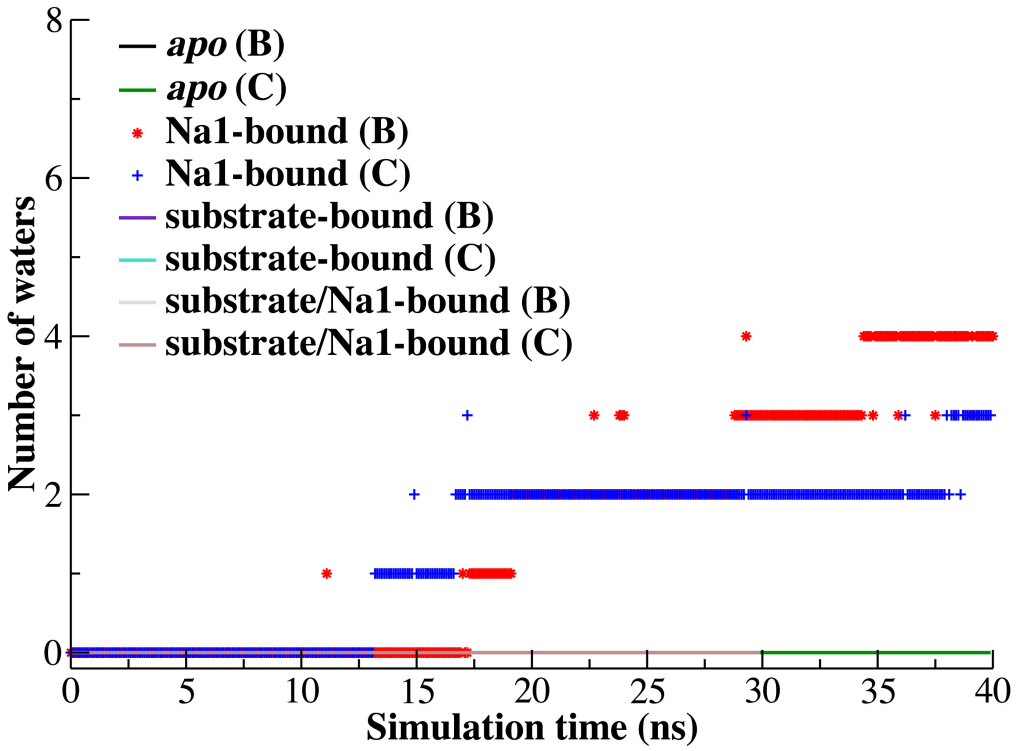

Figure S1: Water accessibility of Asp312 in various bound states in the other two monomers (B and C), which are not reported in the main text. Time series of the number of water molecules were calculated with 3.5 Å of the carboxylate groups of Asp312. It is concluded that extracellular water can access Asp312 only in the Na1-bound state.

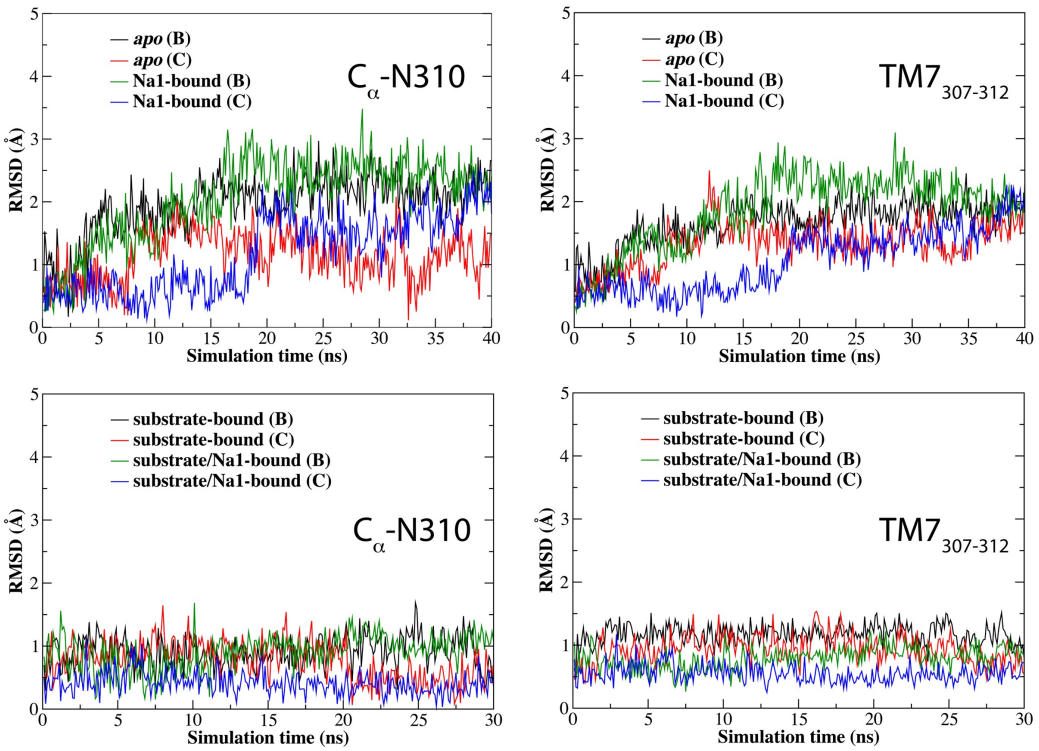

Figure S2: Cα-RMSDs of Asn310 and of $TM7_{307-312}$ (residues 307 to 312) in the various bound states in the other two monomers (B and C), which are not reported in the main text. Consistently, in the *apo* and Na1-bound states in these two monomers, Cα-Asn310 and $TM7_{307-312}$ exhibit large flexibility, however, they display large stability both in the substrate-bound and substrate/Na1-bound states.

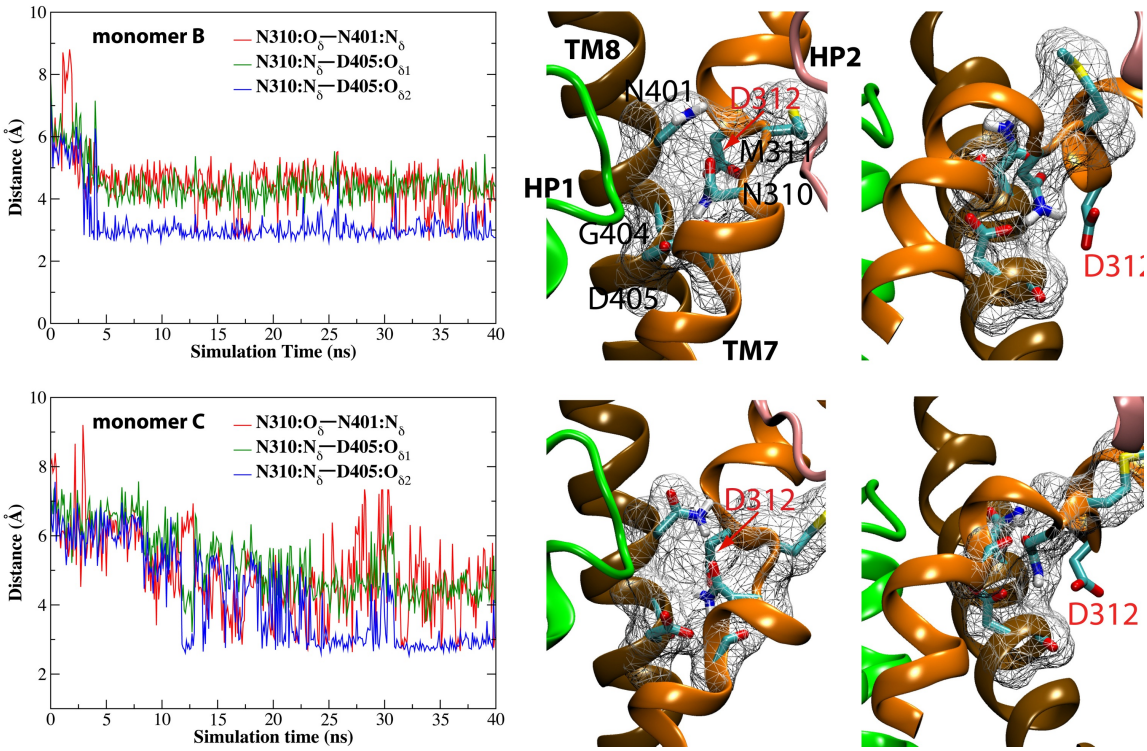

Figure S3: Access of extracellular water to Asp312 is blocked by H-bond network between Asp405, Asn310 and Asn405 in the *apo* state. The two monomers (B and C) are shown here, which are not reported in the main text. (left) Time evolution of the distances between Asn310:O_δ and Asn401:N_δ, and between Asn310:N_δ and Asp405:$O_{\delta 1}$, and between Asn310:N_δ and Asn405:$O_{\delta 2}$ in the two *apo* states. (middle and right) Molecular surface representation of residues Gly306, Asn310, Met311, Asn401, Gly404 and Asp405 in the *apo* states. Middle and right panels show the front and side (90^0-rotated) views, respectively. Clearly, access of extracellular water to Asp312 is completely prevented.

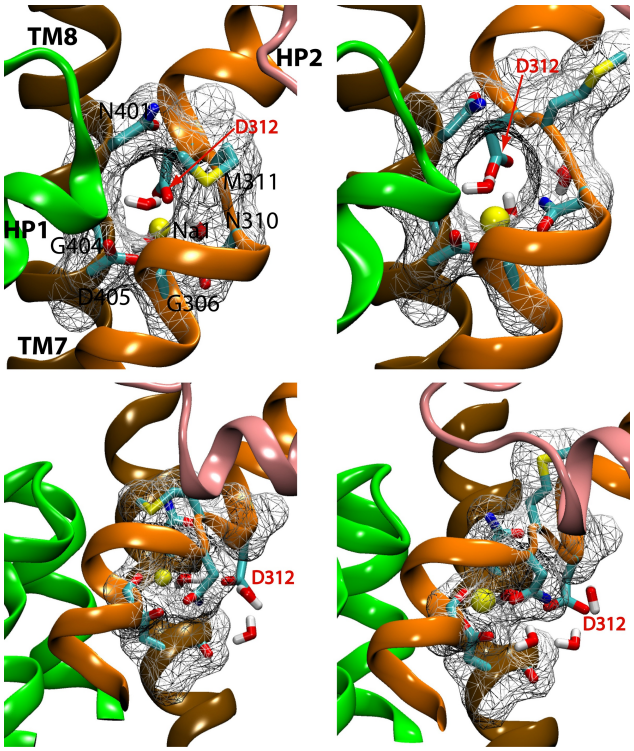

Figure S4: Molecular surface representation of residues Gly306, Asn310, Met311, Asn401, Gly404 and Asp405 in the two Na1-bound states in the other two monomers, which are not reported in the main text. Upper and lower panels show the front and side (90^0-rotated) views, respectively. It is clear that Asp312 can be hydrated in these two Na1-bound states.

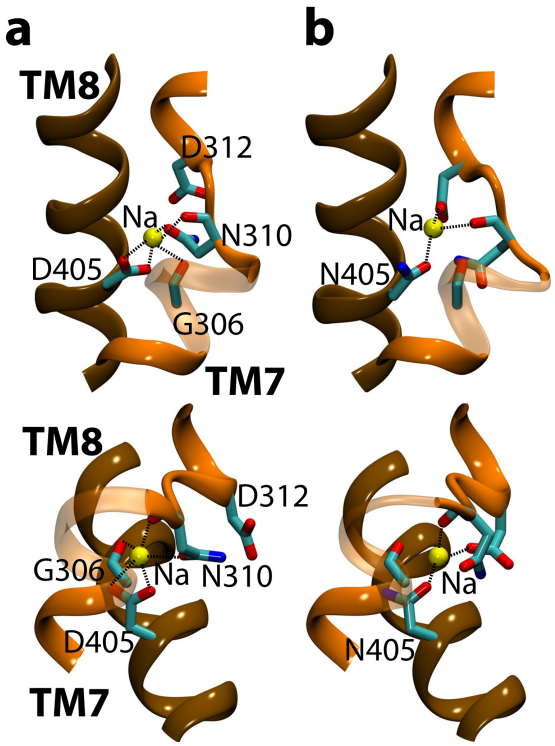

Figure S5: Na^+ in the Na1 site moves toward Asp312 after mutation of Asp405 to asparagine. Upper and lower panels show front and side (90^0-rotated) views, respectively. (a) The last frame of the Na1-bound state showing the Na1 site. (b) Na^+ moves toward Asp312 and is coordinated by Asn310, Asp312 and Asn405 upon mutation of Asp405 to asparagine.

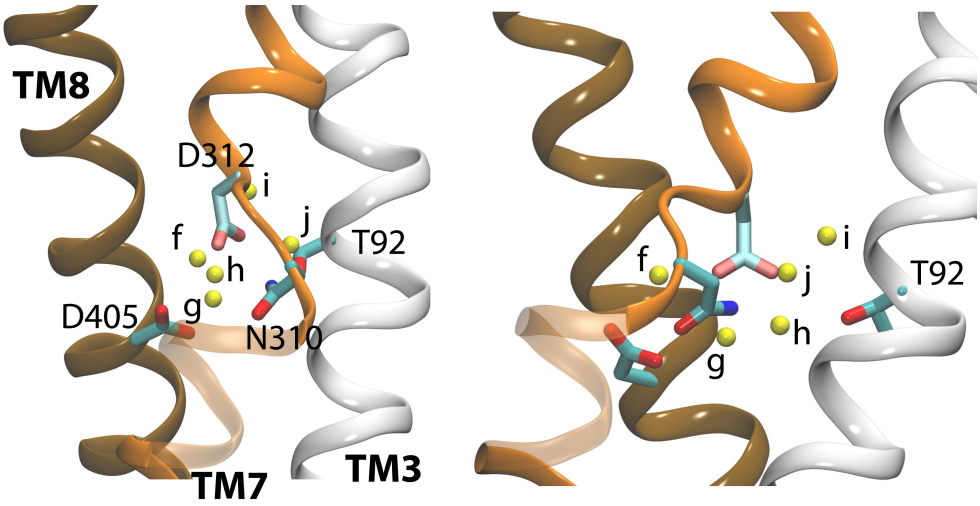

Figure S6: The initial five positions of Na3 in the simulation systems (Na3-f to Na3-j). Left and right show front and side (90^0-rotated) views, respectively.

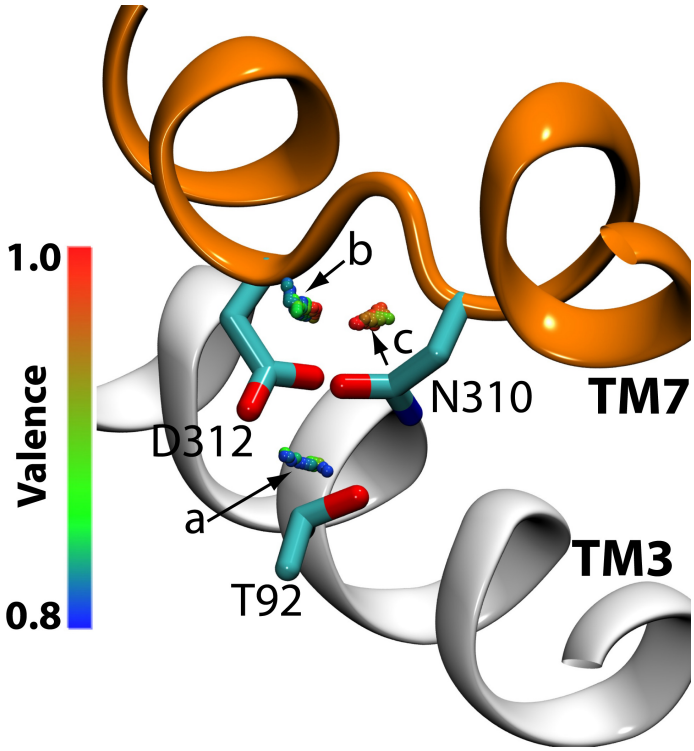

Figure S7: Valence mapping of the crystal structure of Glt_{ph} with aspartate bound (pdb: 2NWX) for Na^+. The dot points with a valence value of 0.8 (blue) to 1.0 (red) inside protein are shown except those nearby Na1 and Na2 binding sites, as indicated by the arrows (a-c). Valence color code is shown on the left side. These dot points (b and c), which are located below the backbone of β-bridge and above the side chains of Asp312 and Asn310, might not indicate a suitable binding site for Na^+, as our simulations show that the placed Na^+ in (b) moves to the intermediate binding site, and the placed Na^+ in (c) moves to the putative Na3 binding site. Therefore, it might be concluded that residues Asn310, Asp312 and Thr92 can form a Na^+ binding site according to the valence mapping calculations.

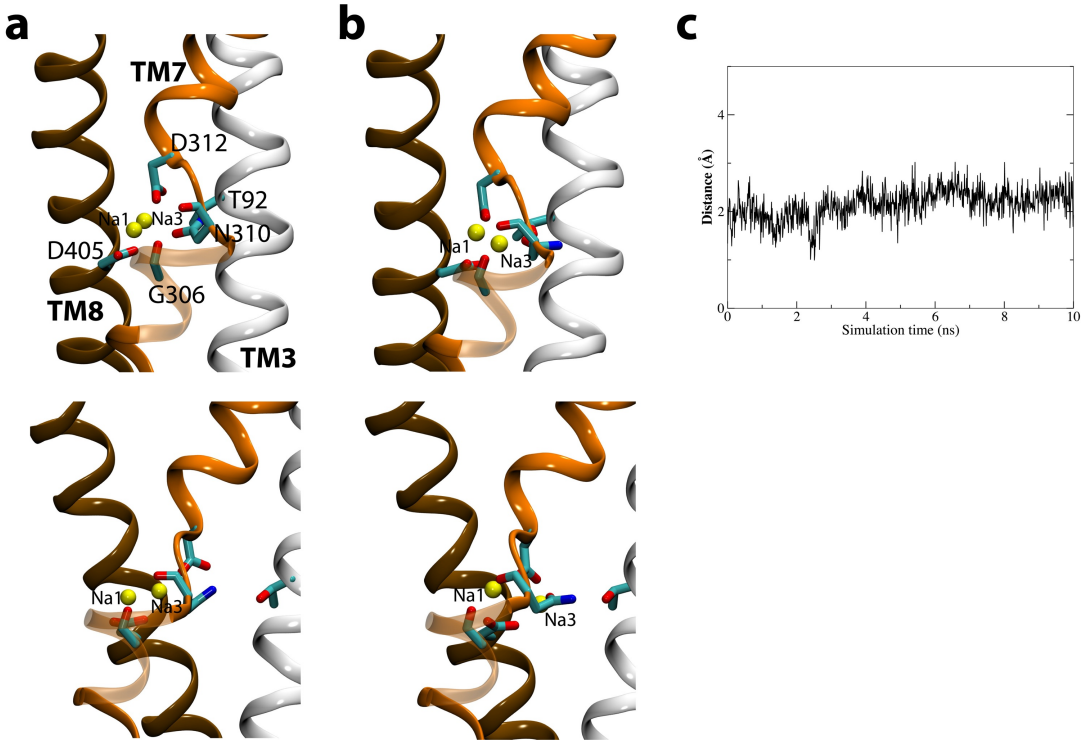

Figure S8: The inward movement of the Na3 in the intermediate binding site upon Na^+ binding to the Na1 binding site. (a and b) The positions of Na1 and Na3 before (a) and after (b) the simulation of the Na1/Na3-bound state, in which Na3 is in the intermediate binding site. Top and down panels show the front and side (90^0-rotated) views, respectively. The Na^+ ion in the intermediate binding site was observed to move deeply down into the protein toward the putative Na3 binding site upon Na1 binding. (c) The displacement of Na3 from its initial position upon the binding of Na1.

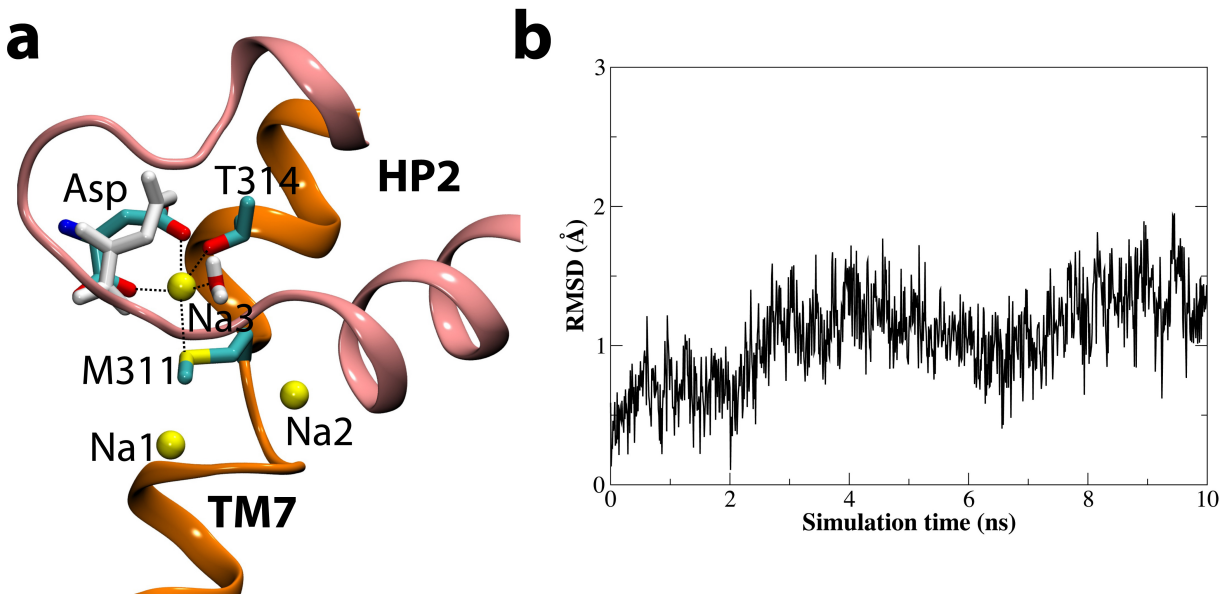

Figure S9: (a) The location of the placed Na^+ in the third Na^+ binding site proposed by Holley et al after equilibration simulation, in which one Na^+ was placed into this proposed site in the aspartate/Na1/Na2-bound state of outward-facing Glt_{ph}. This placed Na^+ is coordinated by the two carboxylate groups of the substrate, and residues Met311 and Thr314 as well as one water molecule, finally. The original location of the substrate aspartate in the crystal structure shown in white. The location of aspartate after equilibration simulation shown in color. (b) The displacement of Cα-substrate from its original position along the simulation time.

References

[1] Boudker, O., R. M. Ryan, D. Yernool, K. Shimamoto, and E. Gouaux. 2007. Coupling substrate and ion binding to extracellular gate of a sodium-dependent aspartate transporter. *Nature*. 445:387–393.

[2] Humphrey, W., A. Dalke, and K. Schulten. 1996. VMD – Visual Molecular Dynamics. *J. Mol. Graphics*. 14:33–38.

[3] Zhang, L. and J. Hermans. 1996. Hydrophilicity of cavities in proteins. *Proteins: Struct., Func., Gen.* 24:433–438.

[4] Grubmüller, H. 1996. SOLVATE 1.0 manual. Theoretical Biophysics Group, Institut für Medizinische Optik, Ludwig-Maximilians-Universität München, München, Germany. http://www.mpibpc.mpg.de/home/grubmueller/downloads/solvate/index.html.

[5] Lomize, M. A., A. L. Lomize, L. D. Pogozheva, and H. I. Mosberg. 2006. Opm: Orientations of proteins in membranes database. *Bioinformatics*. 22:623–625. http://opm.phar.umich.edu/.

[6] Phillips, J. C., R. Braun, W. Wang, J. Gumbart, E. Tajkhorshid, E. Villa, C. Chipot, R. D. Skeel, L. Kale, and K. Schulten. 2005. Scalable molecular dynamics with NAMD. *J. Comp. Chem.* 26:1781–1802.

[7] Jorgensen, W. L., J. Chandrasekhar, J. D. Madura, R. W. Impey, and M. L. Klein. 1983. Comparison of simple potential functions for simulating liquid water. *J. Chem. Phys.* 79:926–935.

[8] MacKerell, A. D., Jr., D. Bashford, M. Bellott, R. L. Dunbrack, Jr., J. D. Evanseck, M. J. Field, S. Fischer, J. Gao, H. Guo, S. Ha, D. Joseph, L. Kuchnir, K. Kuczera, F. T. K. Lau, C. Mattos, S. Michnick, T. Ngo, D. T. Nguyen, B. Prodhom, I. W. E. Reiher, B. Roux, M. Schlenkrich, J. Smith, R. Stote, J. Straub, M. Watanabe, J. Wiorkiewicz-Kuczera, D. Yin, and M. Karplus. 1998. All-atom empirical potential for molecular modeling and dynamics studies of proteins. *J. Phys. Chem. B*. 102:3586–3616.

[9] MacKerell Jr., A. D., M. Feig, and C. L. Brooks III. 2004. Extending the treatment of backbone energetics in protein force fields: Limitations of gas-phase quantum mechanics in reproducing protein conformational distributions in molecular dynamics simulations. *J. Comp. Chem.* 25:1400–1415.

[10] Martyna, G. J., D. J. Tobias, and M. L. Klein. 1994. Constant pressure molecular dynamics algorithms. *J. Chem. Phys.* 101:4177–4189.

[11] Feller, S. E., Y. H. Zhang, R. W. Pastor, and B. R. Brooks. 1995. Constant pressure molecular dynamics simulation — the Langevin piston method. *J. Chem. Phys.* 103:4613–4621.

[12] Darden, T., D. York, and L. Pedersen. 1993. Particle mesh Ewald. An N·log(N) method for Ewald sums in large systems. *J. Chem. Phys.* 98:10089–10092.

[13] Huang, Z. and E. Tajkhorshid. 2008. Dynamics of the extracellular gate and ion-substrate coupling in the glutamate transporter. *Biophys. J.* 95:2292–2300.

[14] Grewer, C., P. Balani, C. Weidenfeller, T. Bartusel, Z. Tao, and T. Tauen. 2005. Individual subunits of the glutamate transporter EAAC1 homotrimer function independently of each other. *Biochemistry.* 44:11913–11923.

[15] Koch, H. P., R. L. Brown, and H. P. Larsson. 2007. The glutamate-activated anion conductance in excitatory amino acid transporter is gated independently by the individual subunits. *J. Neurosci.* 27:2943–2947.

[16] Tao, Z., Z. Zhang, and C. Grewer. 2006. Neutralization of the aspartic acid residue Asp-367, but not Asp-454, inhibits binding of Na^+ to the glutamate-free form and cycling of the glutamate transporter EAAC1. *J. Biol. Chem.* 281:10263–10272.